

# Solvation and Oxidation Effects on the Crystal Structure and Morphology of Tetraoxolene-Based Materials

Journal:	CrystEngComm
Manuscript ID	CE-ART-09-2024-000921.R1
Article Type:	Paper
Date Submitted by the Author:	18-Oct-2024
Complete List of Authors:	Kamin, Ashlyn; University of Washington, Chemistry Brannan, EJ; University of Washington, Chemisry Snook, Kathleen; University of Washington Krajewski, Sebastian; University of Washington, Chemistry Gannon, Paige; University of Washington Kaminsky, Werner; University of Washington, Chemistry Xiao, Dianne; University of Washington, Chemistry

SCHOLARONE™ Manuscripts

# **ARTICLE**

Received 00th January 20xx, Accepted 00th January 20xx

DOI: 10.1039/x0xx000000x

# Solvation and Oxidation Effects on the Crystal Structure and Morphology of Tetraoxolene-Based Materials

Ashlyn A. Kamin,<sup>‡,a</sup> EJ Brannan,<sup>‡,a</sup> Kathleen M. Snook,<sup>a</sup> Sebastian Krajewski,<sup>a</sup> Paige M. Gannon,<sup>a</sup> Werner Kaminsky,<sup>a</sup> Dianne J. Xiao<sup>\*,a</sup>

Owing to their rich redox behavior and strong metal chelating ability, tetraoxolene ligands have been established as one of the foundational building blocks for multifunctional metal–organic materials. Here, we show how simple and often overlooked synthetic parameters can be used to control the structures of transition metal and lanthanide-based metal–tetraoxolene materials across multiple length scales. Through the synthesis of twelve new compounds, we provide a comprehensive survey detailing how the choice of solvent, initial ligand redox state, and *in situ* oxidant impact the local coordination geometry and chain architecture, as well as the crystal size and shape (*e.g.*, rods vs. platelets). This work represents an important step towards the synthesis of new metal–tetraoxolene materials with predictable architectures and, therefore, targeted functionality.

#### Introduction

Tetraoxolene ligands, such as 1,4-dihydroxybenzoquinone and its derivatives, are important building blocks for constructing multifunctional metal—organic materials, boasting multiple stable redox states (**Fig. 1a**), chemical stability, and tunable binding geometries.<sup>1,2</sup> These ligands have been used to synthesize both porous metal—organic frameworks (MOFs) and nonporous coordination networks with high electrical conductivities,<sup>2–4</sup> stimuli-dependent valence tautomerism,<sup>5,6</sup> and interesting magnetic properties.<sup>2,5–7</sup>

A variety of synthetic factors are known to influence the local geometry, metal–ligand connectivity, and crystal morphology of tetraoxolene-based metal–organic chains. For example, modification of the metal cation identity, 1,8 ligand substituents, 9-11 solvent, 6,12-14 and/or rate of oxidation, 15,16 can result in profound differences in the ligand binding modes, material geometry, crystallite size, and resulting physical properties. Given the large number of variables, rational methods for tuning the coordination and material geometry of metal–tetraoxolene materials are still underdeveloped. In this work, we aimed to understand the synthetic factors that influence structural control of metal–tetraoxolene materials across length scales.

Previously, our lab reported the synthesis of both linear and helical iron–tetraoxolene chains using a sterically bulky

Fig 1. (a) Redox series for the deprotonated tetraoxolene ligands,  $R_2dhbq^{n-}$ . Solvent and oxidant effects on the chain structure and crystal morphology of materials formed by combining  $H_4Ph_2dhbq$  with (b) transition metal (TM) ions and (c) lanthanide (Ln) ions.

#These authors contributed equally to this work.
Supplementary Information available. CCDC 2373678-2373681. See DOI: 10.1039/x0xx00000x

R<sub>2</sub>dhbq<sup>4-</sup>
R<sub>2</sub>dhbq<sup>3--</sup>
R<sub>2</sub>dhbq<sup>2-</sup>

b

solvent sterics dictate chain geometry

Image: Solvent sterics dictate chain geometry

oxidant dictates particle morphology

helical 1D chains

C

oxidant dictates chain geometry

zig-zag
1D chains

<sup>&</sup>lt;sup>a.</sup> Department of Chemistry, University of Washington, Seattle, Washington 98195. Email: <u>djxiao@uw.edu</u>

ARTICLE Journal Name

terphenyl-based tetraoxolene ligand,  $H_2Ph_2dhbq$  (2,5-dihydroxy-3,6-dipheny-1,4-benzoquinone). These chains could be synthesized under an inert atmosphere with either Fe<sup>II</sup> and the oxidized 1,4-dihydroxybenzoquinone form of the ligand ( $H_2Ph_2dhbq$ ), or with Fe<sup>III</sup> and the fully reduced tetraol ligand ( $H_4Ph_2dhbq$ ). In the case of the linear chain, the use of Fe<sup>III</sup> salts led to oxidative doping. In addition, we found that through subtle adjustment of the coordinating solvent's steric profile, we could predictably control for helical *versus* linear chain geometries and dramatically modulate their electronic and magnetic behavior.

Given our work on iron-tetraoxolene chains, we hypothesized that the structures of other transition metal and lanthanide-based tetraoxolene systems may also display a strong dependence on solvent choice and oxidant identity. Accordingly, we present the synthesis of a series of eight new metal-tetraoxolene chains (Mg, Mn, Co, and Zn) with solventcontrolled linear versus helical geometries, as previously observed with iron (Fig. 1b). We further show that multiple oxidants can be employed for the in situ oxidation of our ligand during synthesis, including air and, for the first time, MnIII cations. The use of Mn<sup>III</sup> leads to a dramatic change in the crystal shape, altering the morphology from long rods to hexagonal platelets (Fig. 1b). Finally, we extend this study to include trivalent lanthanide metals, reporting four new lanthanide structures that reveal oxidant-dependent geometric control between zig-zag 1D chains and 2D networks (Fig. 1c). Together, these results highlight how simple and often overlooked synthetic parameters, including the initial ligand redox state, oxidant identity, and solvent selection, play critical roles in the formation of tetraoxolene-based materials.

# **Results and discussion**

#### Synthesis of transition metal chains

Our lab has previously shown that single crystals of 1D metalorganic chains can be synthesized by reacting Fe<sup>II</sup> salts with the oxidized dihydroxybenzoquinone form of our tetraoxolene ligand (H<sub>2</sub>Ph<sub>2</sub>dhbq) under an inert atmosphere.<sup>6</sup> In these syntheses, the chains adopt either a linear or helical structure based on the steric bulk of the amide solvent. A bulkier solvent such as dimethylacetamide (DMA) favors coordination of the solvent molecules in a trans geometry and a linear chain whereas structure, a smaller solvent such dimethylformamide (DMF) favors a cis geometry and a helical chain structure. We hypothesized that isostructural chains could be synthesized from alternative transition metals such as manganese. Reactions between manganese(II) nitrate and the oxidized H<sub>2</sub>Ph<sub>2</sub>dhbq in DMA or DMF under an inert atmosphere resulted in the formation of microcrystalline solids composed of poorly defined, intergrown particles as observed by scanning electron microscopy (SEM) (Fig. S13). Employing the preoxidized form of our tetraoxolene ligand likely facilitates rapid nucleation of the chains, leading to a high degree of crystallite intergrowth and small crystallite sizes.

We anticipated that discrete single crystals of our desired chains could be synthesized from Mn<sup>II</sup> and the fully reduced tetraol form of the ligand (H<sub>4</sub>Ph<sub>2</sub>dhbq), utilizing atmospheric oxygen to slowly oxidize the ligand in situ. We found that layering a methanolic solution of manganese(II) nitrate over a solution of H<sub>4</sub>Ph<sub>2</sub>dhbq in DMA in air readily yields diffractionquality single crystals of the linear chain, trans-Mn(Ph<sub>2</sub>dhbq)(DMA)<sub>2</sub>, which were analyzed by single crystal X-Ray diffraction (SCXRD). The crystal structure of trans-Mn(Ph<sub>2</sub>dhbq)(DMA)<sub>2</sub> confirms the presence of six-coordinate manganese nodes that are bound to two axial DMA molecules and bridging bis-bidentate Ph2dhbq2- ligands to form a linear chain structure (Fig. 2a). The bite angle of the tetraoxolene ligands results in moderately compressed equatorial O-Mn-O bond angles of 75.42(7)° within each Mn(Ph₂dhbq) chelate ring, while the axial bond angles average 90(6)°, overall giving rise to a quasi-octahedral metal geometry. As hypothesized, the local chain structure also closely resembles that of trans-Fe(Ph<sub>2</sub>dhbq)(DMA)<sub>2</sub>.<sup>6</sup> Indexing and unit cell refinement of trans-Mn(Ph<sub>2</sub>dhbq)(DMA)<sub>2</sub> reveal a primitive monoclinic lattice and space group of P 2<sub>1</sub>/c. Bond length analysis reveals an average equatorial Mn-O bond length of 2.151(9) Å, consistent with Mn<sup>II</sup> nodes in similar coordination environments.<sup>13</sup> Accordingly, an average tetraoxolene C-O bond length of 1.2615(17) Å demonstrates that the ligands are oxidized to the expected Ph<sub>2</sub>dhbq<sup>2-</sup> oxidation state.<sup>1</sup>

Switching to the less sterically encumbered amide solvent, we find that layering a methanolic solution of manganese(II) nitrate over a solution of H<sub>4</sub>Ph<sub>2</sub>dhbq in DMF in air yields single crystals of the helical chain, cis-Mn(Ph2dhbq)(DMF)2, which were analyzed by SCXRD using a synchrotron X-ray source. The resulting data shows that the manganese sites remain quasioctahedral, but the bridging Ph2dhbq2- ligands and DMF molecules now coordinate cis to one another, prompting the chains to adopt a helical configuration (Fig. 2a). The structure also closely matches cis-Fe(Ph2dhbq)(DMF)2, with an identical trigonal crystal system and P 3<sub>1</sub> space group, as well as similar unit cell parameters. Like the linear chain, bond length analysis of cis-Mn(Ph<sub>2</sub>dhbq)(DMF)<sub>2</sub> is consistent with Mn<sup>II</sup> and Ph<sub>2</sub>dhbq<sup>2-</sup> oxidation states, with an average manganesetetraoxolene Mn-O bond length of 2.119(18) Å and an average tetraoxolene C-O bond length of 1.242(17) Å. Following cis-Fe(Ph<sub>2</sub>dhbq)(DMF)<sub>2</sub>, this represents the second report of a chiral 1D chain synthesized from 1,4-dihydroxybenzoguinone or any of its substituted derivatives.

While the aforementioned layering procedures facilitate the formation of the largest single crystals, we found that heating manganese(II) nitrate and  $H_4Ph_2dhbq$  in either neat DMA or DMF in the presence of air also give rise to single crystals of *trans*-Mn(Ph<sub>2</sub>dhbq)(DMA)<sub>2</sub> and *cis*-Mn(Ph<sub>2</sub>dhbq)(DMF)<sub>2</sub>. This heating procedure is more readily scaled, and the PXRD patterns match the calculated patterns from the single crystal structures of *trans*-Mn(Ph<sub>2</sub>dhbq)(DMA)<sub>2</sub> and *cis*-Mn(Ph<sub>2</sub>dhbq)(DMF)<sub>2</sub> (see **Figs. S9–10**). However, we do observe a notable reduction in crystal size. In the case of *trans*-Mn(Ph<sub>2</sub>dhbq)(DMA)<sub>2</sub>, we see a reduction in average crystal length from 80.3  $\pm$  75.2  $\mu$ m to 28.8  $\pm$  14.6  $\mu$ m when switching

Journal Name ARTICLE

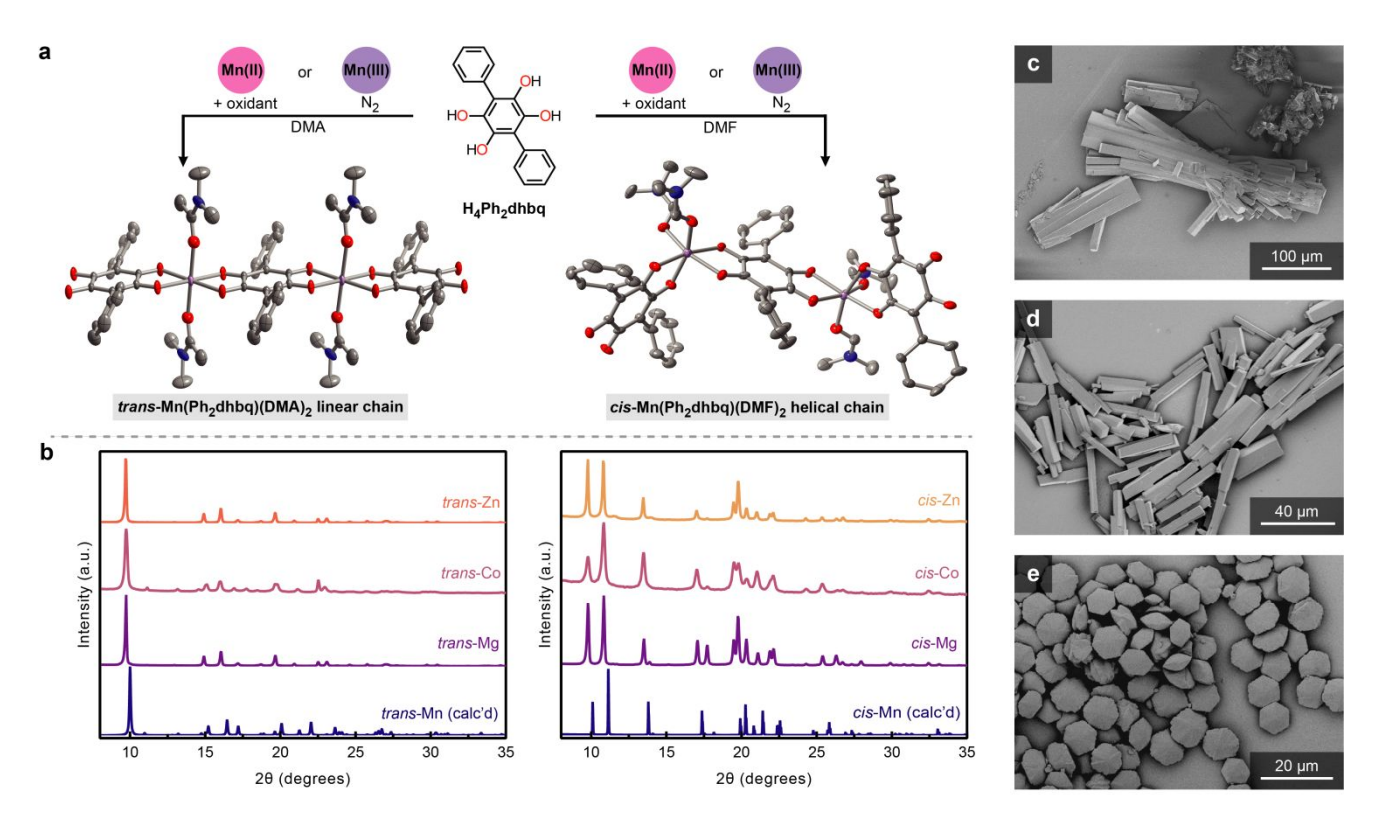


Fig 2. (a) Synthetic scheme and single crystal structures of *trans*-Mn(Ph<sub>2</sub>dhbq)(DMA)<sub>2</sub> and *cis*-Mn(Ph<sub>2</sub>dhbq)(DMF)<sub>2</sub>. Thermal ellipsoids are rendered at the 50% probability level. Mn, C, N, and O atoms are represented by purple, grey, blue, and red, respectively. Hydrogen atoms have been omitted for clarity. (b) PXRD patterns for linear (left) and helical (right) transition metal chains compared to the calculated PXRD patterns of *trans*-Mn(Ph<sub>2</sub>dhbq)(DMA)<sub>2</sub> and *cis*-Mn(Ph<sub>2</sub>dhbq)(DMF)<sub>2</sub>, respectively. SEM images of *trans*-Mn(Ph<sub>2</sub>dhbq)(DMA)<sub>2</sub> synthesized from (c) Mn<sup>III</sup> in layered MeOH/DMA at room temperature in air, (d) Mn<sup>III</sup> in DMA with heating in air, and (e) Mn<sup>III</sup> in DMA with heating under an inert atmosphere.

from the layered to the heated synthetic procedure (**Figs. 2c–d**). In the case of *cis*-Mn(Ph<sub>2</sub>dhbq)(DMF)<sub>2</sub>, we see a reduction in average crystal length from 38.7  $\pm$  18.2  $\mu$ m to 22.9  $\pm$  7.6  $\mu$ m between the layered and heated procedures (**Figs. S14–15**).

Given the pronounced effect of the initial ligand redox state and oxidant identity on crystallite size, we wondered if we could finely calibrate the crystal morphology by employing alternative chemical oxidants under an inert atmosphere. We hypothesized that Mn<sup>III</sup> ions could act as both an in situ oxidant and metal source during synthesis, similar to our previous chain syntheses using  $Fe^{III.6}$  Indeed, we found that heating  $Mn(acac)_3$  ( $acac^{1-}$  = acetylacetonate) with the reduced H<sub>4</sub>Ph<sub>2</sub>dhbq in DMA or DMF yields microcrystalline solids, and the PXRD patterns match the calculated patterns from the single crystal structures of trans- $Mn(Ph_2dhbq)(DMA)_2$  and cis- $Mn(Ph_2dhbq)(DMF)_2$  (Figs. S9–10). Unexpectedly, the crystals synthesized using Mn<sup>III</sup> have dramatically different aspect ratios than the long rods formed in air. The trans-Mn(Ph2dhbq)(DMA)2 chain instead adopts a hexagonal platelet morphology (Fig. 2e), with an average diameter of 8.97  $\pm$  1.32  $\mu m$  and thickness of 4.66  $\pm$  0.87  $\mu m.$  The cis-Mn(Ph<sub>2</sub>dhbq)(DMF)<sub>2</sub> chain forms short rod-like crystals (Fig. **S16**), with an average diameter of 17.6  $\pm$  4.4  $\mu$ m and thickness of  $15.2 \pm 5.9 \,\mu\text{m}$ . We note that this result may be relevant for the morphological control of oxolene-based MOFs, a topic that has received heightened attention given the impact of crystal morphology on mass and charge transport. 17,18

Having demonstrated that both manganese and iron salts readily give rise to single crystals of our desired metal–

tetraoxolene chains, we anticipated that isostructural chains could be accessed with other transition metals. Screening reactions in DMA with other first-row transition metals such as Co and Zn, and alkaline earth metals such as Mg, we found that in all cases we could readily obtain microcrystalline solids with PXRD patterns that closely resembled *trans*-Mn(Ph<sub>2</sub>dhbq)(DMA)<sub>2</sub> (**Fig. 2b**). Pawley refinement of the unit cell dimensions further confirmed the similarity in structure (**Table S5**). Similar reactions in DMF with Co, Zn, and Mg also yielded microcrystalline solids that resembled *cis*-Mn(Ph<sub>2</sub>dhbq)(DMF)<sub>2</sub> by PXRD, which was further confirmed via Pawley refinement (**Fig. 2b** and **Table S6**).

#### Synthesis of lanthanide chains and coordination networks

It has previously been shown that metal–tetraoxolene MOFs can be synthesized from lanthanide ions, and the resulting structures can differ from their transition metal–tetraoxolene counterparts due to the increased ionic radius and capacity for expanded coordination numbers.<sup>8,19–22</sup> As such, we hypothesized that Ln<sup>III</sup> metal ions might allow us to access metal–organic chains akin to those reported with H<sub>4</sub>Ph<sub>2</sub>dhbq and later-period alkaline earth metals,<sup>23,24</sup> as well 2D phases akin to those more recently observed with Ln<sup>III</sup> and bulky *tert*-butyl substituted tetraoxolene ligands.<sup>25</sup>

We found that heating a solution of neodymium(III) nitrate with the reduced  $H_4Ph_2dhbq$  in DMF under an inert atmosphere affords diffraction-quality single crystals of a neodymium—

ARTICLE Journal Name

tetraoxolene chain with the formula Nd(Ph<sub>2</sub>dhbq)(DMF)<sub>3</sub>(NO<sub>3</sub>). To the best of our knowledge, this is the first report of a 1D lanthanide chain synthesized from 1,4-dihydroxybenzoquinone or its substituted derivatives.

The structure of Nd(Ph<sub>2</sub>dhbq)(DMF)<sub>3</sub>(NO<sub>3</sub>) reveals a zig-zag chain geometry with nine-coordinate metal centers bound to two bridging bis-bidentate Ph<sub>2</sub>dhbq<sup>2-</sup> ligands, one bidentate nitrate anion, and three oxygen-coordinated DMF molecules (Fig. 3a). Bond length analysis confirms an average Nd–O bond length of 2.443(19) Å between the metal center and tetraoxolene ligands, which is consistent with the expected Nd-O bond length of 2.51(9) Å for nine-coordinate Nd<sup>III</sup>.<sup>26</sup> We also observe an average tetraoxolene C-O bond length of 1.260(3) Å, again demonstrating the successful in situ oxidization of our ligand to the desired  $Ph_2dhbq^{2-}$  state. It is unclear if this ligand oxidation is facilitated by the nitrate counterions or adventitious oxygen. However, we note that reactions with neodymium(III) chloride under otherwise identical reaction conditions yielded no solid products, even after weeks of heating, suggesting the nitrate counterion is necessary for chain formation. We also note that preliminary PXRD data suggests the same structure can be obtained by heating neodymium(III) nitrate with pre-oxidized H<sub>2</sub>Ph<sub>2</sub>dhbq in DMF under an inert atmosphere, but with a smaller crystallite size (Fig. S11).

Given the similar reactivity across the lanthanide series, we proposed that isostructural analogs of

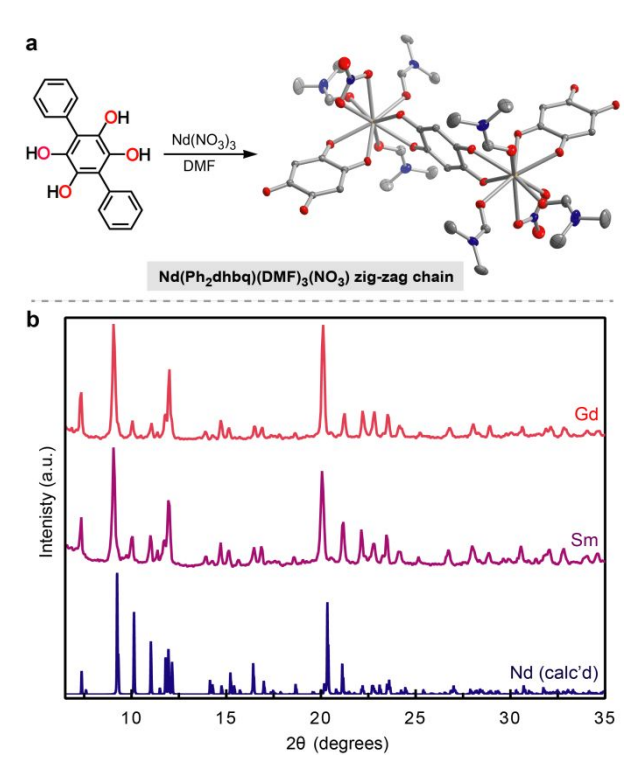
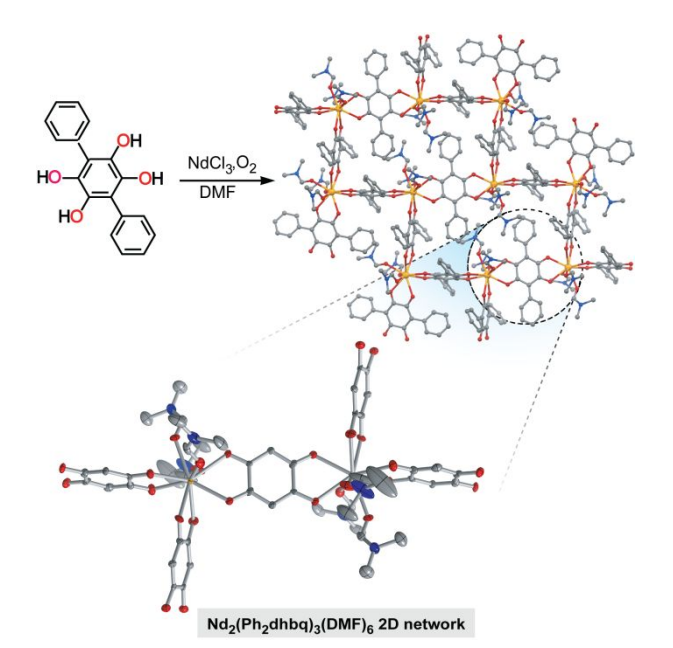


Fig 3. (a) Synthetic scheme and single crystal structure for  $Nd(Ph_2dhbq)(DMF)_2(NO_3)$  zig-zag chains. Thermal ellipsoids are rendered at the 50% probability level. Nd, C, N, and O atoms are represented by yellow, grey, blue, and red, respectively. Hydrogen atoms and tetraoxolene phenyl substituents have been omitted for clarity. (b) PXRD patterns of isostructural Gd and Sm chains in comparison to the calculated PXRD pattern of  $Nd(Ph_2dhbq)(DMF)_3(NO_3)$ .

Nd(Ph<sub>2</sub>dhbq)(DMF)<sub>2</sub>(NO<sub>3</sub>) could be synthesized using alternative lanthanide(III) nitrate salts. While La, Tb, Tm, and Yb yielded either no solid products or microcrystalline solids with unidentifiable PXRD patterns, Sm and Gd both yielded small single crystals with PXRD patterns that matched the calculated pattern of Nd(Ph<sub>2</sub>dhbq)(DMF)<sub>2</sub>(NO<sub>3</sub>), indicating that we can access 1D zig-zag chains from at least three different lanthanide precursors (**Fig. 3b**). Pawley refinements were carried out to determine precise unit cell dimensions of the Sm and Gd analogues, which are tabulated in **Table S7**.

Preliminary attempts to modulate the neodymium chain structure using DMA proved unsuccessful. Heating a solution of neodymium(III) nitrate with  $H_4Ph_2dhbq$  in DMA resulted only in the formation of an amorphous precipitate. Given that there are three solvent molecules per metal center in  $Nd(Ph_2dhbq)(DMF)_3(NO_3)$ , it is possible that the incorporation of three DMA molecules per neodymium is too sterically demanding to yield a crystalline chain structure.

Surprisingly, attempts to synthesize Nd chains using slow aerial oxidation led to the formation of a new phase. The reaction between neodymium(III) nitrate and reduced  $H_4Ph_2dhbq$  in the presence of air afforded a microcrystalline solid with a PXRD pattern that did not match that of  $Nd(Ph_2dhbq)(DMF)_3(NO_3)$ . Subsequent reactions between neodymium(III) chloride and reduced  $H_4Ph_2dhbq$  in the presence of air afforded single crystals of a 2D coordination network with the formula,  $Nd_2(Ph_2dhbq)_3(DMF)_6$ , which were analyzed by SCXRD (**Fig. 4**). The calculated PXRD pattern from this structure appears to match the preliminary PXRD pattern from the reaction with neodymium(III) nitrate and reduced  $H_4Ph_2dhbq$  in air, allowing us to retroactively identify that



**Fig 4.** Synthetic scheme and resulting single crystal structure of the 2D coordination network with the formula  $Nd_2(Ph_2dhbq)_3(DMF)_6$ . Nd, C, N, and O atoms are represented by yellow, grey, blue, and red, respectively. Hydrogen atoms have been omitted for clarity. In the magnified portion of the structure, ellipsoids are rendered at the 50% probability level and tetraoxolene phenyl substituents have been omitted for clarity.

Journal Name ARTICLE

material to be  $Nd_2(Ph_2dhbq)_3(DMF)_6$  (Fig. S12).

SCXRD data for Nd<sub>2</sub>(Ph<sub>2</sub>dhbq)<sub>3</sub>(DMF)<sub>6</sub>, collected using a synchrotron X-ray source, reveals nine-coordinate neodymium metal centers, each with three bis-bidentate bridging Ph<sub>2</sub>dhbq<sup>2-</sup> ligands and three oxygen-bound DMF solvent molecules. The structure is composed of zig-zag chains cross-linked by additional Ph<sub>2</sub>dhbq<sup>2-</sup> ligands to form 2D sheets within the crystallographic ac plane. The interlayer spacing is relatively large due to the steric bulk of the ligand's phenyl substituents, measuring 14.668(7) Å between neodymium atoms on adjacent sheets. The average neodymium-tetraoxolene Nd-O bond length of 2.47(4) Å is consistent with oxygen-bound NdIII. Additionally, the tetraoxolene ligand is fully oxidized to the expected Ph<sub>2</sub>dhbq<sup>2-</sup> state, as confirmed by an average C-O bond length of 1.265(14) Å. The formation of this 2D phase highlights the sensitivity of lanthanide-tetraoxolene materials to the initial ligand redox state and oxidant identity.

#### **Conclusions**

In summary, we have shown that the choice of solvent, initial ligand redox state, and *in situ* oxidant strongly impacts the underlying structure and overall crystal morphology of tetraoxolene-based extended materials. In the context of firstrow transition metals, we have seen that small changes in solvent sterics dramatically modulate the chain geometry between linear and helical. Perhaps the most surprising finding is the sensitivity of the crystal morphology to the choice of oxidant. For manganese chains, the use of air *versus* Mn<sup>III</sup> as the *in-situ* oxidant dramatically changes the crystal shape, from long rods to hexagonal platelets.

While the structure of lanthanide-tetraoxolene materials appear to be less sensitive to solvent sterics, they are highly sensitive to oxidant identity, often in an unpredictable manner. For example, changing the ligand redox state and oxidant identity modulates between the formation of 1D chains *versus* 2D coordination networks. Similar sensitivity has been previously observed in iron—oxolene materials, where either 2D or 3D coordination networks are obtained depending on the initial redox state of the ligand.<sup>27</sup> Together, these results emphasize the importance of canvassing multiple ligand redox states, oxidant combinations, and solvent identities to fully understand the rich phase space of tetraoxolene-based materials.

# **Experimental**

The tetraoxolene ligands, H<sub>2</sub>Ph<sub>2</sub>dhbq and H<sub>4</sub>Ph<sub>2</sub>dhbq, were synthesized as previously reported.<sup>6</sup> The synthesis of all other materials are described in detail in the Supporting Information. Powder X-ray diffraction (PXRD) data were collected on a Bruker D2 PHASER benchtop diffractometer. Standard single-crystal X-ray diffraction (SCXRD) data were collected on a Bruker APEX II single crystal diffractometer with a Mo radiation source. Synchrotron SCXRD data were collected at Beamline 12.2.1 at the Advanced Light Source, Lawrence Berkeley National Lab.

Additional details, including details regarding the solution and refinement of SCXRD data, are described in the Supporting Information.

### **Author contributions**

AAK and DJX designed the research; AAK, EJB, and DJX wrote the manuscript; AAK and EJB carried out the synthesis and routine characterization; SK, PMG, and WK collected and refined the crystallographic data; KMS collected and analyzed the SEM data. All authors interpreted the results and contributed to reviewing and editing the manuscript.

#### **Conflicts of interest**

There are no conflicts to declare.

# Data availability

Additional experimental data supporting this article are included in the ESI.

All crystal structures have been deposited in the Cambridge Crystallographic Data Centre (CCDC) under deposition numbers 2373678-2373681.

# Acknowledgements

This work was supported primarily by the U.S. Department of Energy, Office of Science, Office of Basic Energy Sciences under Award Number DE-SC0021966. The work on lanthanide-based materials was supported by the Arnold and Mabel Beckman Foundation through a Beckman Young Investigator Award. AAK was supported by an NSF graduate research fellowship and UW Clean Energy Institute graduate fellowship. EJB was supported by a Washington Research Foundation undergraduate fellowship and Mary Gates research scholarship. The X-ray facility at the UW Department of Chemistry is supported by NSF Award Number CHE-0840520. The Molecular Analysis Facility at UW is supported in part by the National Science Foundation under Award Number NNCI-1542101. This research also utilized the Advanced Light Source, which is a DOE Office of Science User Facility under Contract Number DE-AC02-05CH11231; we thank Dr. Simon Teat and Dr. Nick Settineri for their assistance with the collection of synchrotron single crystal X-ray diffraction data.

# **Notes and references**

- (1) Kitagawa, S.; Kawata, S. Coordination Compounds of 1,4-Dihydroxybenzoquinone and Its Homologues. Structures and Properties. Coordination Chemistry Reviews 2002, 224 (1), 11–34. https://doi.org/10.1016/S0010-8545(01)00369-1.
- (2) Mercuri, M. L.; Congiu, F.; Concas, G.; Sahadevan, S. A.
  Recent Advances on Anilato-Based Molecular Materials with
  Magnetic and/or Conducting Properties. *Magnetochemistry*

ARTICLE Journal Name

- **2017**, *3* (2), 17.
- https://doi.org/10.3390/magnetochemistry3020017.
- (3) Xie, L. S.; Skorupskii, G.; Dincă, M. Electrically Conductive Metal–Organic Frameworks. Chem. Rev. 2020, 120 (16), 8536–8580. https://doi.org/10.1021/acs.chemrev.9b00766.
- (4) Darago, L. E.; Aubrey, M. L.; Yu, C. J.; Gonzalez, M. I.; Long, J. R. Electronic Conductivity, Ferrimagnetic Ordering, and Reductive Insertion Mediated by Organic Mixed-Valence in a Ferric Semiquinoid Metal—Organic Framework. *J. Am. Chem. Soc.* 2015, 137 (50), 15703–15711. https://doi.org/10.1021/jacs.5b10385.
- (5) DeGayner, J. A.; Wang, K.; Harris, T. D. A Ferric Semiquinoid Single-Chain Magnet via Thermally-Switchable Metal–Ligand Electron Transfer. *Journal of the American Chemical Society* 2018. https://doi.org/10.1021/jacs.8b03949.
- (6) Kamin, A. A.; Moseley, I. P.; Oh, J.; Brannan, E. J.; Gannon, P. M.; Kaminsky, W.; Zadrozny, J. M.; Xiao, D. J. Geometry-Dependent Valence Tautomerism, Magnetism, and Electrical Conductivity in 1D Iron—Tetraoxolene Chains. *Chem. Sci.* 2023, 14 (15), 4083–4090. https://doi.org/10.1039/D2SC06392A.
- (7) Martínez-Hernández, C.; Benmansour, S.; Gómez García, C. J. Modulation of the Ordering Temperature in Anilato-Based Magnets. *Polyhedron* 2019, 170, 122–131. https://doi.org/10.1016/j.poly.2019.05.034.
- (8) F. Abrahams, B.; Coleiro, J.; Ha, K.; F. Hoskins, B.; D. Orchard, S.; Robson, R. Dihydroxybenzoquinone and Chloranilic Acid Derivatives of Rare Earth Metals. *Journal of the Chemical Society, Dalton Transactions* 2002, 0 (8), 1586–1594. https://doi.org/10.1039/B109296K.
- (9) Milašinović, V.; Jurić, M.; Molčanov, K. Nitrochloranilic Acid: A Novel Asymmetrically Substituted Quinoid Bridging Ligand for Design of Coordination Polymers. CrystEngComm 2021, 23 (11), 2304–2315. https://doi.org/10.1039/D1CE00157D.
- (10) Kabir, Md. K.; Kawahara, M.; Adachi, K.; Kawata, S.; Ishii, T.; Kiaagawa, S. One-Dimensional Manganese Assembled Compounds of Bromanilic Acid and Nitranilic Acid. *Molecular Crystals and Liquid Crystals* 2002, 376 (1), 65–70. https://doi.org/10.1080/713738388.
- (11) Atzori, M.; Benmansour, S.; Mínguez Espallargas, G.; Clemente-León, M.; Abhervé, A.; Gómez-Claramunt, P.; Coronado, E.; Artizzu, F.; Sessini, E.; Deplano, P.; Serpe, A.; Mercuri, M. L.; Gómez García, C. J. A Family of Layered Chiral Porous Magnets Exhibiting Tunable Ordering Temperatures. *Inorg. Chem.* 2013, 52 (17), 10031–10040. https://doi.org/10.1021/ic4013284.
- (12) Abrahams, B. F.; Dharma, A. D.; Dyett, B.; Hudson, T. A.; Maynard-Casely, H.; Kingsbury, C. J.; McCormick, L. J.; Robson, R.; Sutton, A. L.; White, K. F. An Indirect Generation of 1D MII-2,5-Dihydroxybenzoquinone Coordination Polymers, Their Structural Rearrangements and Generation of Materials with a High Affinity for H2, CO2 and CH4. *Dalton Trans.* 2016, 45 (4), 1339–1344. https://doi.org/10.1039/C5DT04095G.
- (13) Dubraja, L. A.; Molčanov, K.; Žilić, D.; Kojić-Prodić, B.; Wenger, E. Multifunctionality and Size of the Chloranilate Ligand Define the Topology of Transition Metal Coordination Polymers. New J. Chem. 2017, 41 (14), 6785–6794. https://doi.org/10.1039/C7NJ01058C.
- (14) Trofimova, O. Y.; Maleeva, A. V.; Arsenyeva, K. V.; Klimashevskaya, A. V.; Yakushev, I. A.; Piskunov, A. V. Glycols in the Synthesis of Zinc-Anilato Coordination Polymers.

- *Crystals* **2022**, *12* (3), 370. https://doi.org/10.3390/cryst12030370.
- (15) Abrahams, B. F.; Lu, K. D.; Moubaraki, B.; Murray, K. S.; Robson, R. X-Ray Diffraction and Magnetic Studies on a Series of Isostructural Divalent Metal Chloranilates with Zigzag Polymeric Chain Structures and on a Dinuclear Iron(III) Chloranilate †. J. Chem. Soc., Dalton Trans. 2000, No. 11, 1793–1797. https://doi.org/10.1039/b000192i.
- (16) Abrahams, B. F.; Hudson, T. A.; McCormick, L. J.; Robson, R. Coordination Polymers of 2,5-Dihydroxybenzoquinone and Chloranilic Acid with the (10,3)- a Topology. Crystal Growth & Design 2011, 11 (7), 2717–2720. https://doi.org/10.1021/cg2005908.
- (17) Snook, K. M.; Zasada, L. B.; Chehada, D.; Xiao, D. J. Oxidative Control over the Morphology of Cu<sub>3</sub> (HHTP)<sub>2</sub>, a 2D Conductive Metal–Organic Framework. *Chem. Sci.* 2022, 13 (35), 10472–10478. https://doi.org/10.1039/D2SC03648G.
- (18) W. Gittins, J.; J. Balhatchet, C.; M. Fairclough, S.; C. Forse, A. Enhancing the Energy Storage Performances of Metal—Organic Frameworks by Controlling Microstructure. *Chemical Science* 2022, *13* (32), 9210–9219. https://doi.org/10.1039/D2SC03389E.
- (19) Nakabayashi, K.; Ohkoshi, S. Monometallic Lanthanoid Assembly Showing Ferromagnetism with a Curie Temperature of 11 K. *Inorg. Chem.* 2009, 48 (18), 8647–8649. https://doi.org/10.1021/ic900625a.
- (20) Demars, T.; Boltoeva, M.; Vigier, N.; Maynadié, J.; Ravaux, J.; Genre, C.; Meyer, D. From Coordination Polymers to Doped Rare-Earth Oxides. *Eur J Inorg Chem* **2012**, *2012* (24), 3875–3884. https://doi.org/10.1002/ejic.201200284.
- (21) Oggianu, M.; Abhervé, A.; Marongiu, D.; Quochi, F.; Galán-Mascarós, J. R.; Bertolotti, F.; Masciocchi, N.; Avarvari, N.; Mercuri, M. L. Terbium and Europium Chlorocyananilate-Based 2D Coordination Polymers. *Molecules* 2023, 28 (18), 6453. https://doi.org/10.3390/molecules28186453.
- (22) Gómez-Claramunt, P.; Benmansour, S.; Hernández-Paredes, A.; Cerezo-Navarrete, C.; Rodríguez-Fernández, C.; Canet-Ferrer, J.; Cantarero, A.; Gómez-García, C. J. Tuning the Structure and Properties of Lanthanoid Coordination Polymers with an Asymmetric Anilato Ligand. Magnetochemistry 2018, 4 (1), 6. https://doi.org/10.3390/magnetochemistry4010006.
- (23) Robl, C.; Kuhs, W. F. Complexes with Substituted 2,5-Dihydroxy-p-Benzoquinones: A Neutron Diffraction Study on BaC6(C6H5)2O4·4H2O. Journal of Solid State Chemistry 1988, 74 (1), 21–26. https://doi.org/10.1016/0022-4596(88)90326-X.
- (24) Robl, C.; Weiss, A. Komplexe mit substituierten 2,5-Dihydroxy-p-benzochinonen: EAC6(C6H5)2O4 · 4 H2O (EA = Sr2+, Ba2+). Zeitschrift für anorganische und allgemeine Chemie 1987, 546 (3), 152–160. https://doi.org/10.1002/zaac.19875460316.
- (25) Kharitonov, A. D.; Trofimova, O. Y.; Meshcheryakova, I. N.; Fukin, G. K.; Khrizanforov, M. N.; Budnikova, Y. H.; Bogomyakov, A. S.; Aysin, R. R.; Kovalenko, K. A.; Piskunov, A. V. 2D-Metal–Organic Coordination Polymers of Lanthanides (La(III), Pr(III) and Nd(III)) with Redox-Active Dioxolene Bridging Ligands. CrystEngComm 2020, 22 (28), 4675–4679. https://doi.org/10.1039/DOCE00767F.
- (26) Gagné, O. C. Bond-Length Distributions for Ions Bonded to Oxygen: Results for the Lanthanides and Actinides and

Journal Name ARTICLE

- Discussion of the f-Block Contraction. *Acta Cryst B* **2018**, *74* (1), 49–62. https://doi.org/10.1107/S2052520617017425.
- (27) Wang, L.; Papoular, R. J.; Horwitz, N. E.; Xie, J.; Sarkar, A.; Campisi, D.; Zhao, N.; Cheng, B.; Grocke, G. L.; Ma, T.; Filatov, A. S.; Gagliardi, L.; Anderson, J. S. Linker Redox Mediated Control of Morphology and Properties in Semiconducting Iron-Semiquinoid Coordination Polymers\*\*. *Angew Chem Int Ed* 2022, 61 (45). https://doi.org/10.1002/anie.202207834.

The data supporting this article have been included as part of the Supplementary Information.

All crystal structures have been deposited in the Cambridge Crystallographic Data Centre (CCDC) under deposition numbers 2373678-2373681.